RSC Medicinal Chemistry

ROYAL SOCIETY OF CHEMISTRY

RESEARCH ARTICLE

View Article Online
View Journal | View Issue

Cite this: *RSC Med. Chem.*, 2025, **16**, 6059

Discovery of a first-in-class SLIT2 binder disrupting the SLIT2/ROBO1 axis *via* DNA-encoded library (DEL) screening

Shaoren Yuan,[a] Somaya A. Abdel-Rahman,[ab] Nelson García Vázquez,[a] Hossam Nada,[a] Laura Calvo-Barreiro,[a] Katarzyna Kuncewicz[ac] and Moustafa T. Gabr *[a]

Received 22nd June 2025,
Accepted 28th September 2025

DOI: 10.1039/d5md00555h

rsc.li/medchem

The SLIT2/ROBO1 signaling axis plays a critical role in neural development, immune regulation, and tumor progression, including glioblastoma. However, small molecule inhibitors targeting this protein–protein interaction remain unexplored. Herein, we report the discovery and validation of **DEL-S1**, a first-in-class small molecule that binds to SLIT2 and disrupts its interaction with ROBO1. Using a DNA-encoded library (DEL) screen of 4.2 billion compounds, **DEL-S1** was identified and confirmed to bind SLIT2 *via* temperature-related intensity change (TRIC) assay. Functional inhibition of the SLIT2/ROBO1 complex by **DEL-S1** was demonstrated using a time-resolved fluorescence resonance energy transfer (TR-FRET) assay, yielding an IC_{50} of 68.8 ± 12.5 μM. Molecular docking and molecular dynamics (MD) simulations revealed key interaction hotspots at the SLIT2 binding interface and confirmed that **DEL-S1** impairs SLIT2/ROBO1 complex formation by inducing conformational rearrangements. **DEL-S1** exhibited favorable ADME properties, including satisfactory plasma and microsomal stability, low cytotoxicity, and minimal hERG liability. To facilitate structure–activity relationship (SAR) exploration, we designed and implemented a modular, one-pot synthetic route leveraging cyanuric chloride reactivity, enabling rapid derivatization of the triazine scaffold of **DEL-S1**. This strategy yielded structurally diverse analogs, including water-soluble carboxylate derivatives with preserved SLIT2/ROBO1 inhibitory activity. Together, this work establishes a novel chemical scaffold targeting SLIT2 and introduces a flexible synthetic platform to support further optimization toward therapeutic development.

Introduction

Slit guidance ligands (SLITs) are glycoproteins that control axon guidance and neuronal migration, through binding to ROBO (Roundabout) receptors.[1] In mammals, the SLIT family —comprising SLIT1, SLIT2, and SLIT3—binds to the immunoglobulin-like domain 1 (Ig1) of ROBO1 and ROBO2 *via* the D2 domain, a conserved leucine-rich repeat region.[2,3] Beyond their classical role in axonal guidance, SLIT2/ROBO1 signaling is now recognized as a multifaceted regulator of physiological and pathological processes, including organ morphogenesis, cellular homeostasis, and tumor biology. This pathway not only orchestrates cellular motility and polarity but also modulates apoptosis, adhesion, and angiogenic responses, partly through downstream effectors like PI3K/Akt and various cytoskeletal adaptors.[3–5]

SLIT2/ROBO signaling mediates axonal repulsion in the developing central nervous system by activating intracellular pathways that remodel the cytoskeleton and redirect axonal extension.[6,7] It also influences the migratory behavior of neurons[8] and guides axonal growth and pathfinding.[9] Beyond neurodevelopment, SLIT proteins exert diverse effects on immune cell trafficking. They function as chemoattractants for neutrophils while simultaneously repelling lymphocytes and dendritic cells, thereby creating cell type-specific patterns of immune cell positioning.[10–12] In macrophages, SLIT2 modulates functional states by reducing macropinocytic activity and dampening the acquisition of pro-inflammatory or cytotoxic phenotypes.[13] SLIT2 promotes vascular sprouting by directing tip cell alignment and migration, especially in retinal and skeletal tissues.[14–16]

In oncogenesis, SLIT2 functions in a context-dependent manner, exerting both tumor-promoting and tumor-restraining effects depending on the tissue and microenvironment. In several cancers—including colorectal,

[a] *Department of Radiology, Molecular Imaging Innovations Institute (MI3), Weill Cornell Medicine, New York, NY 10065, USA. E-mail: mog4005@med.cornell.edu*
[b] *Department of Medicinal Chemistry, Faculty of Pharmacy, Mansoura University, Mansoura 35516, Egypt*
[c] *Department of Biomedical Chemistry, Faculty of Chemistry, University of Gdansk, Poland*

pancreatic, and osteosarcoma—SLIT2 is implicated in promoting invasive behaviors,[17] supporting metastatic dissemination,[18–21] and mediating resistance to therapy.[22] However, in certain epithelial tumors such as breast and lung cancer, SLIT2/ROBO signaling is more often associated with growth inhibition and metastasis suppression.[23–25] The role of this pathway in glioblastoma (GBM) remains particularly complex: while some studies indicate tumor-inhibitory properties,[26–28] others highlight a pro-tumorigenic role,[29,30] suggesting that its biological effects are highly dependent on the cellular context and tumor ecosystem. A growing body of evidence highlights SLIT2/ROBO signaling as a mechanism of immune suppression in the GBM tumor microenvironment (TME).[31] Functional experiments have demonstrated that either silencing SLIT2 in glioma cells or blocking it systemically using a decoy receptor (ROBO1Fc) reduces TAM polarization and angiogenic gene signatures in preclinical GBM models.[31]

Despite these promising findings, clinical exploration of SLIT2/ROBO-targeted therapies remains limited. A protein therapeutic targeting this pathway, PF-06730512, was evaluated in patients with focal segmental glomerulosclerosis (FSGS), but the trial (NCT03448692) was terminated due to insufficient efficacy at tolerable doses.[32,33] Furthermore, several ongoing trials (NCT03940820, NCT03941457, NCT03931720) are investigating ROBO1-directed CAR-NK cell therapies for solid tumors. Compared to biologics, small molecules offer several pharmacological advantages: reduced immunogenicity, improved control of exposure, and often favorable oral bioavailability.[34–37] Their shorter systemic persistence also lowers the risk of extended on-target toxicities.[38,39] Despite this, small molecule inhibitors of the SLIT2/ROBO1 axis are largely unexplored, representing a critical gap in the therapeutic landscape. The limitations of biologics—including restricted tissue penetration, manufacturing complexity, and potential immune activation—further underscore the need for small-molecule alternatives.[34–39] Targeted small molecule-based therapies could provide a scalable and adaptable approach to disrupt SLIT2-mediated immune evasion and tumor progression, particularly in challenging cancers such as GBM.

We recently developed a high-throughput TR-FRET assay for the SLIT2/ROBO1 interaction, enabling for the first time the discovery of small molecule inhibitors targeting this pathway.[40] Although the TR-FRET assay detects SLIT2/ROBO1 binding, directly targeting SLIT2 can disrupt upstream signaling, potentially yielding inhibitors with improved specificity and functional efficacy, thereby overcoming limitations of assays focused solely on protein–protein proximity. DNA-encoded library (DEL) technology has emerged as a transformative approach for the discovery of small molecule ligands capable of reversible target engagement, dramatically expanding the scope of chemical diversity beyond what is accessible through conventional high-throughput screening (HTS).[41–46] By linking small molecules to unique DNA tags that serve as molecular barcodes, DEL platforms enable the construction and interrogation of libraries containing millions to billions of distinct entities.[41,42] Screening is performed under pooled conditions, using minute amounts of the immobilized protein of interest. High-affinity binders are selectively retained on the target while nonspecific compounds are eliminated through washing. The retained molecules are then identified *via* DNA sequencing, which decodes the attached barcodes and enables rapid hit identification.[41–43]

In the present study, we applied DEL screening to discover novel small molecule binders targeting SLIT2, with the goal of disrupting its interaction with ROBO1. Our workflow for this study is presented in Fig. 1. Starting from a DEL-derived hit, we confirmed its ability to bind SLIT2 using biophysical screening assays. We then demonstrated its capacity to inhibit the SLIT2/ROBO1 interaction using our recently reported TR-FRET assay[40] for SLIT2/ROBO1 inhibition. Structural modeling of the SLIT2 binding interface and molecular dynamics (MD) simulations revealed key interaction hotspots, offering valuable guidance for future analog design and structure–activity relationship (SAR) studies. Remarkably, we evaluated the key pharmacokinetics (PK) and physicochemical properties of the DEL hit to inform future optimization efforts. Finally, we developed a synthetic route for the DEL hit, enabling the generation of an analog library to probe the structural features critical for SLIT2 binding. Given the limited number of successful applications of DEL technology to protein–protein interactions involved in immune regulation, our work underscores the potential of this platform to identify

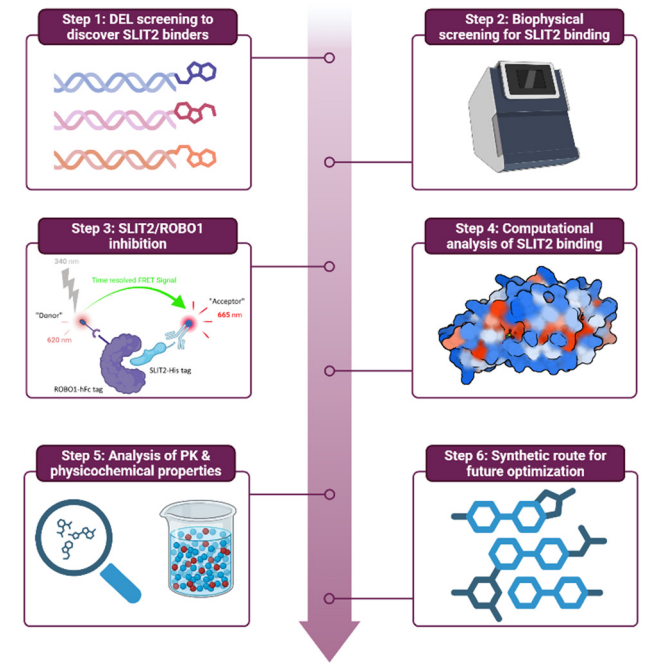

Fig. 1 Workflow for the discovery of small molecule SLIT2 binders as inhibitors of SLIT2/ROBO1 interaction.

first-in-class SLIT2-targeted small molecules that inhibit SLIT2/ROBO1 interaction.

Results and discussion

DEL screening

The DELopen kit is a publicly accessible DEL platform from WuXi AppTec that enables academic labs to perform affinity-based selections on diverse chemical matter without proprietary constraints. It includes structurally diverse libraries designed to broadly sample chemical space across multiple pharmacophores and scaffolds. A DEL screening of 4.2 billion compounds from the DELopen kit (WuXi AppTec) against the human SLIT2 protein resulted in the identification of 3481 full-length compounds spanning 20 of the 27 included libraries (data not shown). Selection criteria included filtering out NTC signals (C4) from target conditions (C1, C2, and C3), applying an enrichment score threshold of 100, and prioritizing compounds that exhibited exclusive binding to the SLIT2 protein (A area) (Fig. 2A). This multistep filtering process allowed us to eliminate false positives and emphasize selective SLIT2 engagement. Distinct enrichment patterns emerged from multiple libraries, and based on these trends (Fig. 2B), along with the most prevalent chemotypes identified in the data analysis, the top small molecule SLIT2 binder (**DEL-S1**, Fig. 2C) was selected for further investigation. Subsequently, we procured **DEL-S1** from WuXi AppTec (purity >95%, see Fig. S1–S5 for NMR, LCMS, mass spectra, HPLC purity, and chiral supercritical fluid chromatography (SFC)) to validate its potential to bind SLIT2 and inhibit key SLIT2 interactions.

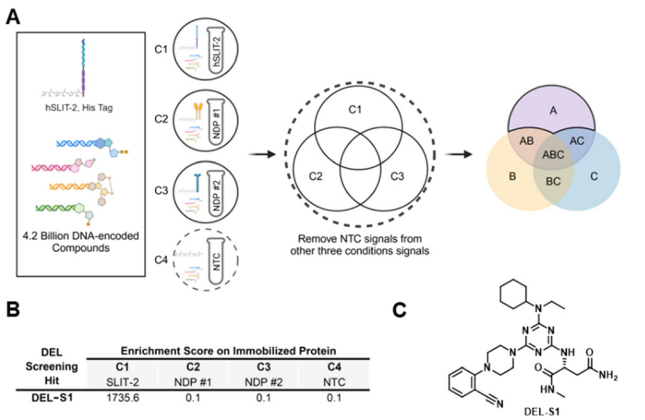

Fig. 2 Identification of the top small molecule SLIT2 binder *via* DEL screening. (A) A total of 27 DNA-encoded libraries, encompassing 4.2 billion compounds, were screened against human SLIT2 protein immobilized on HisPur™ Ni-NTA magnetic beads (C1), along with two undisclosed human proteins immobilized on the same affinity matrix (C2, C3), and a non-target control (NTC, C4) consisting of the affinity matrix alone. Following affinity selection, bound small molecules were sequenced to decode their DNA tags. Compounds detected in area A, after filtering out NTC signals (C4) and applying selection criteria, were identified as potential SLIT2 binders. (B) Enrichment scores of **DEL-S1**, the top-selected small molecule binder for human SLIT2 following affinity selection. (C) Chemical structure of **DEL-S1**. Abbreviations: DEL, DNA-encoded library; NDP, non-disclosed protein.

Biophysical validation

To validate **DEL-S1** as a first-in-class SLIT2-binding small molecule, we employed temperature-related intensity change (TRIC), a solution-phase biophysical technique that quantifies compound–protein interactions based on fluorescence changes under thermal gradients. Recombinant SLIT2 protein was fluorescently labeled and incubated with increasing concentrations of **DEL-S1**. The resulting thermophoretic signal demonstrated a clear, concentration-dependent response, consistent with a specific binding event (Fig. 3). The observed TRIC signal suggests that **DEL-S1** engages SLIT2 in its native conformation, under near-physiological buffer conditions, without the need for immobilization or labeling of the compound. This is particularly valuable for protein–protein interaction targets like SLIT2, which often present shallow and dynamic binding surfaces that are challenging to interrogate using conventional biophysical approaches. Taken together, these results establish **DEL-S1** as a validated small molecule binder of SLIT2 and support its advancement into functional inhibition assays designed to probe its ability to disrupt the SLIT2/ROBO1 interaction.

TR-FRET for SLIT2/ROBO1 inhibition

In order to validate **DEL-S1** as a SLIT2 binder capable of disrupting its functional interaction with ROBO1, we employed our previously optimized TR-FRET assay[40] designed to quantify SLIT2/ROBO1 complex formation. In this system, d2-labeled SLIT2 and terbium-labeled ROBO1 were incubated in the presence of increasing concentrations of **DEL-S1**. In the absence of compound, a strong TR-FRET signal was observed, reflecting stable interaction between SLIT2 and ROBO1 (Fig. 4). Titration of **DEL-S1** resulted in a concentration-dependent decrease in TR-FRET efficiency, consistent with inhibition of the SLIT2/ROBO1 interaction. Nonlinear regression analysis of the dose–response curve yielded an IC_{50} value of 68.8 ± 12.5 μM (Fig. 4), indicating the inhibitory activity of **DEL-S1** against this protein–protein

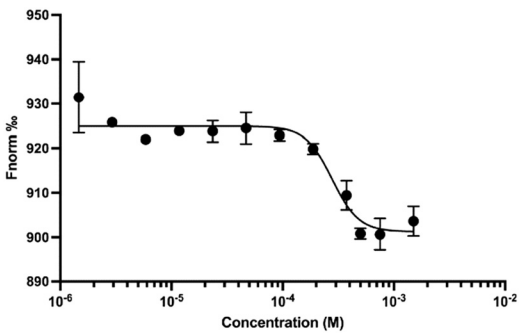

Fig. 3 Dose-dependent curve for the binding of **DEL-S1** (12 assay points, 1.5 mM–1.5 μM, 2-fold dilution) to SLIT2 using TRIC.

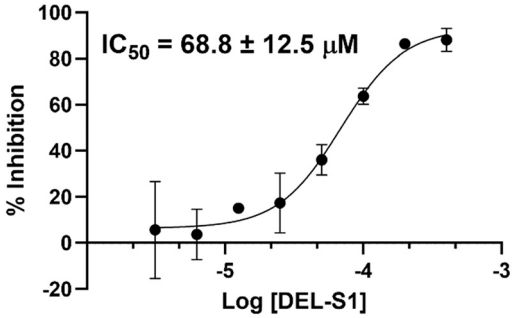

Fig. 4 Dose-dependent curve for the inhibition of SLIT2/ROBO1 interaction by **DEL-S1** using TR-FRET assay. Error bars represent standard deviation (n = 3).

interaction. Control experiments confirmed that the reduction in TR-FRET signal was not due to fluorescence quenching or compound interference with assay components. These findings establish **DEL-S1** as a functional small molecule inhibitor of the SLIT2/ROBO1 axis, underscoring its promise as a scaffold for therapeutic development in diseases such as glioblastoma.

Computational analysis of the SLIT2 binding site

To better understand how our lead compound interacts with SLIT2 and guide future optimization efforts, we performed a detailed computational analysis of the SLIT2 binding site. This structural insight was aimed at identifying key molecular hotspots within the SLIT2 D2 domain that mediate its interaction with the ROBO1 Ig1 domain. The molecular interaction between ROBO1 and SLIT2 is mediated through a series of interactions between the Ig1 domain of ROBO1 and the concave face of the SLIT2 D2 domain.[47] This ROBO1/SLIT2 interaction involves two distinct binding regions (Fig. 5A): an electrostatic interface formed by salt bridges (involving Ig1 residues Glu-72 and Lys-90 and SLIT2 D2 residues Arg-306 and Glu-304) and hydrogen bonds two hydrogen bonds (involving Asn-88 and Ser-75 of Ig1 and Arg-328 and Arg-287 of SLIT2 D2) between specific loops and strands, and a hydrophobic interface (involving Val-354, Ala-381, Leu-376, Leu-378, Leu-400, Ser-402, Tyr-404, His-426, and Ser-453)[47] characterized by extensive apolar contacts between β-strand clusters (Fig. 5B).

Induced fit docking (IFD) was employed to dock **DEL-S1** into the protein–protein interaction interface of SLIT2. The IFD protocol in Maestro (Schrödinger) was specifically used to account for the conformational flexibility of the SLIT2 binding site during ligand accommodation. The resulting binding pose of **DEL-S1** (Fig. 5C and D) revealed that the compound established five hydrogen bonds with key residues in region 1 of the SLIT2 interface, namely Arg306, Glu308, Arg328, Asp330, and Ser352. In addition to these polar interactions, **DEL-S1** formed hydrophobic π–π stacking and van der Waals interactions with Tyr356, Leu376, and Leu378, which are part of region 2 (Fig. 5A). Collectively, these interactions suggest that **DEL-S1** is capable of engaging both critical regions of the SLIT2/ROBO binding interface, potentially disrupting their association and explaining the compound's observed inhibitory activity.

To evaluate the effect of **DEL-S1** binding on the SLIT2/ROBO interaction, a ternary complex comprising SLIT2, **DEL-S1**, and ROBO was constructed and analyzed (Fig. 6A–C). The ternary complex showed that **DEL-S1** binding to SLIT2 significantly disrupted the native SLIT2/ROBO1 protein–protein interface, leading to a notable reduction in both the

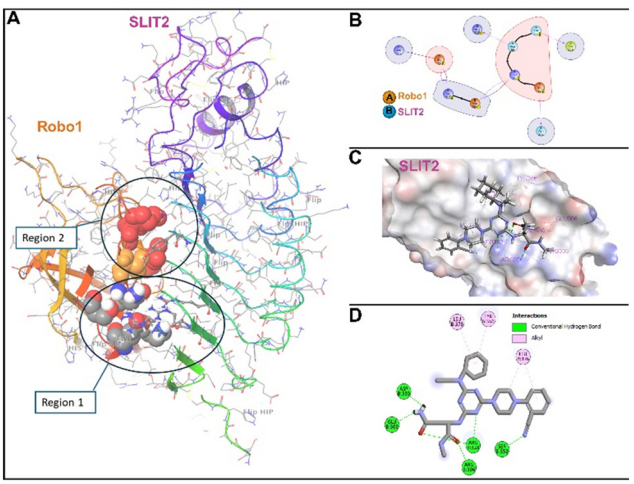

Fig. 5 (A) The SLIT2/ROBO binding interface (PDB ID: 2V9T). (B) Interaction diagram illustrating key residue-level contacts within the native SLIT2/ROBO1 interface. (C) Three-dimensional binding pose of **DEL-S1** at the SLIT2 protein–protein interaction surface, showing occupancy of the ROBO1-binding pocket. (D) Two-dimensional interaction diagram of the **DEL-S1**/SLIT2 complex. Hydrogen bonds are depicted as dashed green lines, while π–π stacking interactions are shown in pink.

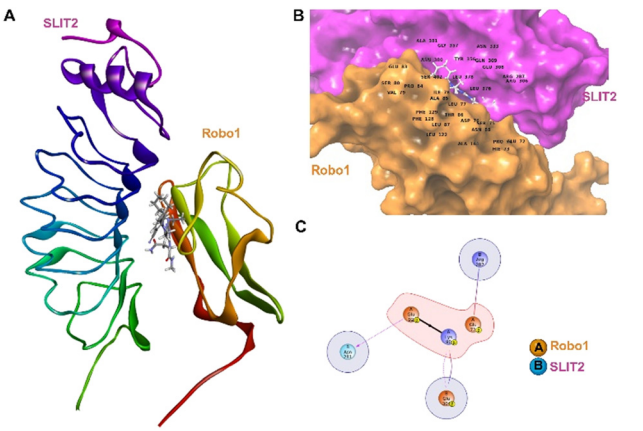

Fig. 6 Effect of **DEL-S1** binding on the SLIT2–ROBO1 interaction. (A) Modeled ternary complex of **DEL-S1**-bound SLIT2–ROBO1, illustrating the spatial arrangement of all three components. (B) Three-dimensional surface representation of the ternary complex, highlighting the altered interaction interface upon **DEL-S1** binding. (C) 2D interaction diagram showing key residue-level contacts within the **DEL-S1**-bound SLIT2–ROBO1 interface, indicating the reduced and redistributed binding interactions compared to the native complex.

complexity and extent of intermolecular contacts. The number of stabilizing contacts between SLIT2 and ROBO1 in the ternary complex was significantly reduced, with only a limited subset of residues remaining engaged (Fig. 6C). In the **DEL-S1**-bound state, the interaction is primarily maintained through ROBO residues Glu-92, Glu-72, and Lys-90, interacting with SLIT2 residues Arg-287, Glu-304, and Asn-281. This represented a substantial loss of interface complexity compared to the native conformation, indicating that **DEL-S1** binding either induces conformational rearrangements in SLIT2 that misalign critical contact residues or directly competes with ROBO1 for overlapping binding sites.

A 100 ns MD simulation was performed to assess the stability of the predicted **DEL-S1**/SLIT2 complex and its effect on the SLIT2/ROBO interaction. Throughout the MD simulation, **DEL-S1** remained stably bound to SLIT2 and was able to consistently maintain the hydrogen bond interaction with Arg328. In contrast, the distance between SLIT2 and ROBO1 progressively increased (Fig. 7) over the course of the simulation which resulted in hindering ROBO1 from forming its native and residue-specific contacts within the canonical SLIT2/ROBO1 interface. Together, these observations explain the observed inhibitory activity of **DEL-S1** on the SLIT2/ROBO1 interaction.

An important consideration for future development is the selectivity of **DEL-S1** across the SLIT family and their ROBO partners. Although **DEL-S1** was identified from a DEL screen that prioritized SLIT2 binding, we have not yet assessed activity against SLIT1, SLIT3, or ROBO2. Structural modeling indicates that **DEL-S1** engages unique features of the SLIT2 D2 domain, including Arg306, Arg328, and Tyr356, which may serve as selectivity determinants. Ongoing efforts will expand biophysical and functional assays to SLIT1/SLIT3 and ROBO2, ensuring that optimization of this chemotype yields ligands with precise SLIT2/ROBO1 targeting.

Assessment of the key PK and physicochemical properties of DEL-S1

The development of small molecule therapeutics for cancer, particularly brain cancers, requires not only inhibition of disease-relevant pathways but also favorable PK and safety profiles that support effective drug delivery to the central nervous system (CNS). To evaluate the suitability of **DEL-S1** as a preliminary hit for CNS-targeted therapy, we performed a comprehensive *in vitro* ADME (absorption, distribution, metabolism, and excretion) assessment using standardized assay protocols (Table 1).

Kinetic solubility of **DEL-S1** was measured at 246 μM, demonstrating acceptable aqueous solubility under physiologically relevant conditions. This parameter is particularly important for CNS-active drugs, as it enables sufficient free drug concentration in systemic circulation. This was further supported by its balanced log*P* of 1.63 (Table 1). The compound's PAMPA (parallel artificial

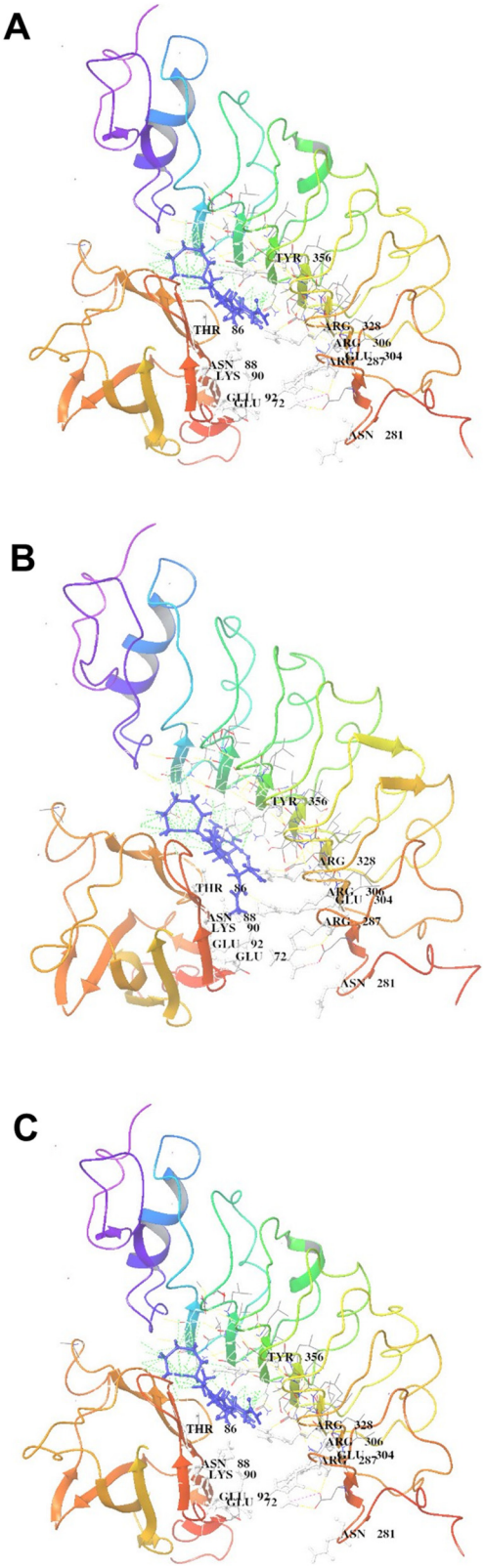

Fig. 7 Conformational changes in the SLIT2–ROBO1 ternary complex during a 100 ns molecular dynamics simulation. (A) Snapshot of the initial structure of the ternary complex. (B) Intermediate structure at 50 ns showing partial separation between SLIT2 and ROBO1. (C) Final structure at 100 ns, highlighting a further increase in the distance between SLIT2 and ROBO1, suggesting progressive weakening of their interaction.

Table 1 *In vitro* PK profile of **DEL-S1**

PK property	Value
log $D_{7.4}$ [a]	1.63
Kinetic solubility 1% DMSO/PBS [μM] [b]	246
PAMPA permeability [cm s^{-1}]	2.1×10^{-6}
PPB human [%] [c]	88.2 ± 3.16
$t_{1/2}$ [h] mouse liver microsomes [c]/CL_{int} [d]	1.9 ± 0.4/18 ± 1.4
$t_{1/2}$ [h] human liver microsomes [c]/CL_{int} [d]	2.5 ± 0.3/22 ± 1.2
$t_{1/2}$ [h] mouse plasma	1.7 ± 0.2
$t_{1/2}$ [h] human plasma	2.1 ± 0.3
$t_{1/2}$ [h] PBS	>4
IC_{50} against hERG [μM]	>100

[a] log *D* (pH = 7.4) the distribution coefficient at physiological pH 7.4. [b] Kinetic solubility measured in 1% DMSO/PBS (pH 7.4) by UV-vis spectrophotometry (n = 3). [c] Values are mean ± SD (n = 3). [d] Intrinsic clearance expressed in μL/(min × mg) protein. Values are mean ± SD (n = 3).

membrane permeability assay) permeability was 2.1×10^{-6} cm s^{-1}, consistent with moderate passive diffusion across lipid membranes, likely due to its high polarity. Plasma protein binding (PPB) of **DEL-S1** was measured at 88.2%, indicating a substantial proportion of the compound is bound in circulation, while still allowing a pharmacologically active free fraction.

DEL-S1 exhibited moderate stability in both mouse and human plasma, with half-lives ($t_{1/2}$) of 1.7 ± 0.2 h and 2.1 ± 0.3 h, respectively (Table 1). Microsomal stability assays revealed half-lives of 1.9 ± 0.4 h in mouse and 2.5 ± 0.3 h in human liver microsomes, indicating that **DEL-S1** is not rapidly metabolized and may maintain systemic exposure following administration. The intrinsic clearance (Cl_{int}) was determined to be 18 ± 1.4 mL min^{-1} mg^{-1} (mouse) and 22 ± 1.2 mL min^{-1} mg^{-1} (human), consistent with moderate hepatic metabolism and favorable bioavailability characteristics.

To evaluate off-target cytotoxicity, **DEL-S1** was tested at 50 μM for 72 hours in three representative non-cancerous human cell lines: normal human astrocytes (NHA), human brain microvascular endothelial cells (hBMECs), and HepG2 hepatocytes. As shown in Fig. S6, **DEL-S1** had minimal cytotoxic effects across all three cell types. Cell viability remained above 95% in NHA, hBMECs, and HepG2 cells, supporting a favorable safety profile. *In vitro* hERG liability assessment showed an IC_{50} > 100 μM, suggesting a low risk of cardiotoxicity at therapeutically relevant concentrations (Table 1). Collectively, these findings demonstrate that **DEL-S1** exhibits physicochemical and ADME properties compatible with small molecule drug development. Its balanced metabolic stability, aqueous solubility, passive permeability, and low off-target cytotoxicity render it a promising lead candidate for further hit-to-lead optimization studies.

Synthetic route for optimization studies

To generate a focused analog library of **DEL-S1** for future SAR studies, we employed a modular synthetic strategy

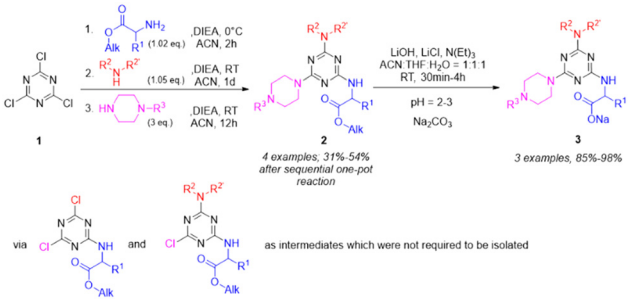

Scheme 1 Synthesis of **DEL-S1** derivatives (**2**) *via* sequential one-pot nucleophilic aromatic substitution and selective hydrolysis products (**3**).

(Scheme 1) leveraging the electrophilic reactivity of cyanuric chloride (**1**), a highly reactive molecule featuring three chlorine atoms that serve as replaceable sites. These chlorine atoms can be sequentially substituted by various nucleophiles under controlled conditions with sequential steps, making cyanuric chloride a versatile scaffold for creating a wide range of triazine derivatives. By adjusting reaction conditions, such as temperature and the order of nucleophile addition, sequential nucleophilic substitutions are achieved in one-pot.

As shown in Scheme 1, amino acid esters were selected as the initial nucleophiles in the reaction sequence, driven by their relatively low nucleophilicity and limited solubility, necessitating the use of the most reactive electrophilic site on the cyanuric chloride scaffold. Conversely, piperazine derivatives, characterized by their high nucleophilic strength, were designated as the final nucleophiles to engage with the mono-chlorinated intermediates, facilitating complete substitution. This sequential arrangement can be adapted based on the nucleophilic properties of the reagents; for instance, the incorporation of highly nucleophilic secondary or primary amines could be adapted as the third reagent added in the synthesis. This step-by-step substitution enables the modular attachment of different substituents to the triazine core, producing a

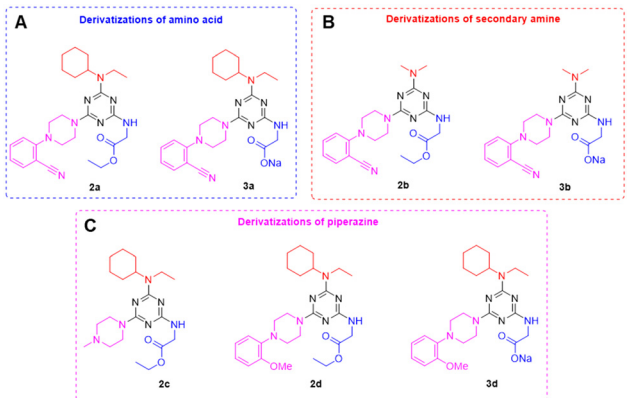

Fig. 8 Chemical structures of the synthesized **DEL-S1** derivatives. (A) The derivatizations of amino acid; (B) the derivatizations of secondary amine; and (C) the derivatizations of piperazine.

library of compounds (**2**, Scheme 1) tailored for SAR studies.

This synthetic platform supports flexible adaptation based on the nucleophilic profile of the input reagents, allowing for rapid diversification of the triazine scaffold with both hydrophobic and polar substituents. As shown in Fig. 8, the synthesized compounds (**2a–d**) included changes in three key fragments of the initial hit (**DEL-S1**). To improve aqueous solubility and PK properties, selected analogs underwent ester hydrolysis (Scheme 1) to yield corresponding carboxylic acid derivatives (**3**). This modification remarkably enhanced the solubility of the resulting **3a**, **3b**, and **3d** compounds (Fig. 8), addressing a key limitation in early-stage drug candidates.

Preliminary evaluation of the synthesized compounds indicated that the ester derivatives (**2a–d**) exhibited limited solubility under the SLIT2/ROBO1 TR-FRET assay conditions, precluding their functional assessment. In contrast, the corresponding sodium carboxylates (**3a**, **3b**, and **3d**) demonstrated improved solubility, allowing for potency evaluation. Notably, compounds **3a** and **3d** possessed SLIT2/ROBO1 inhibitory activity, with IC_{50} values of 225.4 μM and 238.8 μM, respectively. However, compound **3b** lacked inhibitory SLIT2/ROBO1 activity. Although our initial analogs did not exceed the potency of **DEL-S1**, the modular one-pot cyanuric chloride strategy provides a versatile platform for SAR exploration. By systematically varying amino acid-derived side chains and amine substituents, we can probe polar and hydrophobic interactions within the SLIT2 interface to improve binding affinity. In parallel, incorporation of solubilizing groups and optimization of physicochemical properties (*e.g.*, log*P*, polar surface area) will guide CNS penetration, which is essential for GBM applications. The ability to rapidly generate diverse analogs with controlled polarity and lipophilicity underscores the potential of this synthetic strategy to deliver more potent and brain-penetrant inhibitors in future studies.

Although **DEL-S1** exhibits modest potency (IC_{50} = 68.8 ± 12.5 μM) and initial analogs such as **3a** and **3d** are weaker, such values are consistent with first-generation PPI inhibitors. Based on our structural insights, we anticipate potency gains through reinforcing hydrogen bonds with Arg306/Arg328, engaging the hydrophobic Tyr356/Leu376/Leu378 cluster, rigidifying substituents to reduce entropic costs, and leveraging the modular triazine scaffold for fragment-merging and solubilizing modifications. These strategies provide a roadmap for advancing **DEL-S1** into a higher-affinity SLIT2/ROBO1 inhibitor.

Conclusions

In summary, we report the discovery and validation of **DEL-S1** as the first small-molecule binder of SLIT2 capable of disrupting the SLIT2/ROBO1 interaction—a protein–protein interface long considered undruggable. Using a DEL screen of over 4 billion compounds, **DEL-S1** emerged as a selective SLIT2 ligand and was biophysically and functionally validated using TRIC and TR-FRET assays. Computational modeling and molecular dynamics simulations revealed its binding mode and mechanistic disruption of the SLIT2/ROBO1 complex. To accelerate SAR exploration, we established a modular, one-pot synthetic route leveraging cyanuric chloride chemistry, enabling rapid generation of **DEL-S1** analogs. This platform yielded water-soluble derivatives with SLIT2/ROBO1 inhibitory activity, demonstrating the tractability of the chemotype. Moreover, **DEL-S1** showed favorable ADME properties, low cytotoxicity, and low hERG liability, underscoring its potential as a lead for CNS-targeted therapies. Collectively, this work not only identifies a novel chemical probe for the SLIT2/ROBO1 axis but also provides a versatile synthetic toolkit and roadmap for developing next-generation immunomodulatory therapeutics in oncology. A limitation of this study is the absence of cellular efficacy data. Although **DEL-S1** was validated through biophysical and functional assays, future work will extend to cellular models of SLIT2 signaling, including assays of immune modulation and GBM cell migration and invasion. These studies, followed by *in vivo* evaluation in GBM models, will be critical to establish the translational potential of **DEL-S1** and its optimized analogs.

Conflicts of interest

There are no conflicts to declare.

Data availability

Supplementary information: experimental procedures, and supplementary figures. See DOI: **https://doi.org/10.1039/D5MD00555H**.

The authors confirm that all data are available as SI. Furthermore, additional data and original files are available from the authors upon request.

Acknowledgements

We acknowledge funding support by R01CA293456 (PI Gabr) from the National Cancer Institute (NCI).

Notes and references

1 K. Brose, K. S. Bland, K. H. Wang, D. Arnott, W. Henzel, C. S. Goodman, M. Tessier-Lavigne and T. Kidd, Slit proteins bind Robo receptors and have an evolutionarily conserved role in repulsive axon guidance, *Cell*, 1999, **96**, 795–806.

2 R. Barak, G. Yom-Tov, J. Guez-Haddad, L. Gasri-Plotnitsky, R. Maimon, M. Cohen-Berkman, A. A. McCarthy, E. Perlson, S. Henis-Korenblit, M. N. Isupov and Y. Opatowsky, Structural Principles in Robo Activation and Auto-inhibition, *Cell*, 2019, **177**, 272–285.

3 H. Blockus and A. Chédotal, Slit-Robo signaling, *Development*, 2016, **143**, 3037–3044.

4 I. V. Beamish, L. Hinck and T. E. Kennedy, Making Connections: Guidance Cues and Receptors at Nonneural Cell-Cell Junctions, *Cold Spring Harbor Perspect. Biol.*, 2018, **10**, a029165.
5 F. Bisiak and A. A. McCarthy, Structure and Function of Roundabout Receptors, *Subcell. Biochem.*, 2019, **93**, 291–319.
6 R. E. McConnell, J. Edward van Veen, M. Vidaki, A. V. Kwiatkowski, A. S. Meyer and F. B. Gertler, A requirement for filopodia extension toward Slit during Robo-mediated axon repulsion, *J. Cell Biol.*, 2016, **213**, 261–274.
7 H. S. Li, J. H. Chen, W. Wu, T. Fagaly, L. Zhou, W. Yuan, S. Dupuis, Z. H. Jiang, W. Nash, C. Gick, D. M. Ornitz, J. Y. Wu and Y. Rao, Vertebrate slit, a secreted ligand for the transmembrane protein roundabout, is a repellent for olfactory bulb axons, *Cell*, 1999, **96**, 807–818.
8 L. Carr, D. B. Parkinson and X. P. Dun, Expression patterns of Slit and Robo family members in adult mouse spinal cord and peripheral nervous system, *PLoS One*, 2017, **12**, e0172736.
9 H. E. Brown, M. C. Reichert and T. A. Evans, in Vivo Functional Analysis of Drosophila Robo1 Fibronectin Type-III Repeats, *G3*, 2018, **8**, 621–630.
10 D. Pilling, L. E. Chinea, K. M. Consalvo and R. H. Gomer, Different Isoforms of the Neuronal Guidance Molecule Slit2 Directly Cause Chemoattraction or Chemorepulsion of Human Neutrophils, *J. Immunol.*, 2019, **202**, 239–248.
11 A. Prasad, Z. Qamri, J. Wu and R. K. Ganju, Slit-2/Robo-1 modulates the CXCL12/CXCR4-induced chemotaxis of T cells, *J. Leukocyte Biol.*, 2007, **82**, 465–476.
12 S. Tole, I. M. Mukovozov, Y. W. Huang, M. A. Magalhaes, M. Yan, M. R. Crow, G. Y. Liu, C. X. Sun, Y. Durocher, M. Glogauer and L. A. Robinson, The axonal repellent, Slit2, inhibits directional migration of circulating neutrophils, *J. Leukocyte Biol.*, 2009, **86**, 1403–1415.
13 V. K. Bhosle, T. Mukherjee, Y. W. Huang, S. Patel, B. W. F. Pang, G. Y. Liu, M. Glogauer, J. Y. Wu, D. Philpott, S. Grinstein and L. A. Robinson, SLIT2/ROBO1-signaling inhibits macropinocytosis by opposing cortical cytoskeletal remodeling, *Nat. Commun.*, 2020, **11**, 4112.
14 N. Rama, A. Dubrac, T. Mathivet, R. A. Ní Chárthaigh, G. Genet, B. Cristofaro, L. Pibouin-Fragner, L. Ma, A. Eichmann and A. Chédotal, Slit2 signaling through Robo1 and Robo2 is required for retinal neovascularization, *Nat. Med.*, 2015, **21**, 483–491.
15 A. Dubrac, G. Genet, R. Ola, F. Zhang, L. Pibouin-Fragner, J. Han, J. Zhang, J. L. Thomas, A. Chedotal, M. A. Schwartz and A. Eichmann, Targeting NCK-Mediated Endothelial Cell Front-Rear Polarity Inhibits Neovascularization, *Circulation*, 2016, **133**, 409–421.
16 R. Xu, A. Yallowitz, A. Qin, Z. Wu, D. Y. Shin, J. M. Kim, S. Debnath, G. Ji, M. P. Bostrom, X. Yang, C. Zhang, H. Dong, P. Kermani, S. Lalani, N. Li, Y. Liu, M. G. Poulos, A. Wach, Y. Zhang, K. Inoue, A. Di Lorenzo, B. Zhao, J. M. Butler, J. H. Shim, L. H. Glimcher and M. B. Greenblatt, Targeting skeletal endothelium to ameliorate bone loss, *Nat. Med.*, 2018, **24**, 823–833.
17 B. Wang, Y. Xiao, B. B. Ding, N. Zhang, X. Yuan, L. Gui, K. X. Qian, S. Duan, Z. Chen, Y. Rao and J. G. Geng, Induction of tumor angiogenesis by Slit-Robo signaling and inhibition of cancer growth by blocking Robo activity, *Cancer Cell*, 2003, **4**, 19–29.
18 W. J. Zhou, Z. H. Geng, S. Chi, W. Zhang, X. F. Niu, S. J. Lan, L. Ma, X. Yang, L. Wang, Y. Q. Ding and J. G. Geng, Slit-Robo signaling induces malignant transformation through Hakai-mediated E-cadherin degradation during colorectal epithelial cell carcinogenesis, *Cell Res.*, 2011, **21**, 609–626.
19 Q. Q. Zhang, D. L. Zhou, Y. Lei, L. Zheng, S. X. Chen, H. J. Gou, Q. L. Gu, X. D. He, T. Lan, C. L. Qi, J. C. Li, Y. Ding, L. Qiao and L. Wang, Slit2/Robo1 signaling promotes intestinal tumorigenesis through Src-mediated activation of the Wnt/β-catenin pathway, *Oncotarget*, 2015, **6**, 3123–3135.
20 V. Secq, J. Leca, C. Bressy, F. Guillaumond, P. Skrobuk, J. Nigri, S. Lac, M. Lavaut, T. Bui, A. Thakur, N. Callizot, R. Steinschneider, P. Berthezene, N. Dusetti, M. Ouaissi, V. Moutardier, E. Calvo, C. Bousquet, S. Garcia, G. Bidaut, S. Vasseur, J. Iovanna and R. Tomasini, Stromal SLIT2 impacts on pancreatic cancer-associated neural remodeling, *Cell Death Dis.*, 2015, **6**, e1592.
21 B. Tavora, T. Mederer, K. J. Wessel, S. Ruffing, M. Sadjadi, M. Missmahl, B. N. Ostendorf, X. Liu, J. Y. Kim, O. Olsen, A. L. Welm, H. Goodarzi and S. F. Tavazoie, Tumoural activation of TLR3-SLIT2 axis in endothelium drives metastasis, *Nature*, 2020, **586**, 299–304.
22 W. J. Zhou, Z. H. Geng, J. R. Spence and J. G. Geng, Induction of intestinal stem cells by R-spondin 1 and Slit2 augments chemoradioprotection, *Nature*, 2013, **501**, 107–111.
23 A. Dallol, N. F. Da Silva, P. Viacava, J. D. Minna, I. Bieche, E. Maher and F. Latif, SLIT2, a human homologue of the Drosophila Slit2 gene, has tumor suppressor activity and is frequently inactivated in lung and breast cancers, *Cancer Res.*, 2002, **62**, 5874–5880.
24 R. C. Tseng, S. H. Lee, H. S. Hsu, B. H. Chen, W. C. Tsai, C. Tzao and Y. C. Wang, SLIT2 attenuation during lung cancer progression deregulates beta-catenin and E-cadherin and associates with poor prognosis, *Cancer Res.*, 2010, **70**, 543–551.
25 P. H. Chang, W. Hwang-Verslues, Y. C. Chang, C. C. Chen, M. Hsiao, Y. M. Jeng, K. J. Chang, E. Y. Lee, J. Y. Shew and W. H. Lee, Activation of Robo1 signaling of breast cancer cells by Slit2 from stromal fibroblast restrains tumorigenesis via blocking PI3K/Akt/β-catenin pathway, *Cancer Res.*, 2012, **72**, 4652–4661.
26 S. Mertsch, N. Schmitz, A. Jeibmann, J. G. Geng, W. Paulus and V. Senner, Slit2 involvement in glioma cell migration is mediated by Robo1 receptor, *J. Neurooncol.*, 2008, **87**(1), 1–7, DOI: **10.1007/s11060-007-9484-2**.
27 J. J. Yiin, B. Hu, M. J. Jarzynka, H. Feng, K. W. Liu, J. Y. Wu, H. I. Ma and S. Y. Cheng, Slit2 inhibits glioma cell invasion in the brain by suppression of Cdc42 activity, *Neuro Oncol.*, 2009, **11**, 779–789.

28 L. Liu, W. Li, S. Geng, Y. Fang, Z. Sun, H. Hu, Z. Liang and Z. Yan, Slit2 and Robo1 expression as biomarkers for assessing prognosis in brain glioma patients, *Surg. Oncol.*, 2016, **25**, 405–410.

29 V. Amodeo, D. A, J. Betts, S. Bartesaghi, Y. Zhang, A. Richard-Londt, M. Ellis, R. Roshani, M. Vouri, S. Galavotti, S. Oberndorfer, A. P. Leite, A. Mackay, A. Lampada, E. W. Stratford, N. Li, D. Dinsdale, D. Grimwade, C. Jones, P. Nicotera, D. Michod, S. Brandner and P. Salomoni, A PML/Slit Axis Controls Physiological Cell Migration and Cancer Invasion in the CNS, *Cell Rep.*, 2017, **20**, 411–426.

30 F. A. Siebzehnrubl, D. J. Silver, B. Tugertimur, L. P. Deleyrolle, D. Siebzehnrubl, M. R. Sarkisian, K. G. Devers, A. T. Yachnis, M. D. Kupper, D. Neal, N. H. Nabilsi, M. P. Kladde, O. Suslov, S. Brabletz, T. Brabletz, B. A. Reynolds and D. A. Steindler, The ZEB1 pathway links glioblastoma initiation, invasion and chemoresistance, *EMBO Mol. Med.*, 2013, **5**, 1196–1212.

31 L. H. Geraldo, Y. Xu, L. Jacob, L. Pibouin-Fragner, R. Rao, N. Maissa, M. Verreault, N. Lemaire, C. Knosp, C. Lesaffre, T. Daubon, J. Dejaegher, L. Solie, J. Rudewicz, T. Viel, B. Tavitian, S. De Vleeschouwer, M. Sanson, A. Bikfalvi, A. Idbaih, Q. R. Lu, F. R. Lima, J. L. Thomas, A. Eichmann and T. Mathivet, SLIT2/ROBO signaling in tumor-associated microglia and macrophages drives glioblastoma immunosuppression and vascular dysmorphia, *J. Clin. Invest.*, 2021, **131**, e141083.

32 L. H. Beck, S. P. Berasi, J. B. Copley, D. Gorman, D. I. Levy, C. N. Lim, J. M. Henderson, D. J. Salant and W. Lu, PODO: Trial Design: Phase 2 Study of PF-06730512 in Focal Segmental Glomerulosclerosis, *Kidney Int. Rep.*, 2021, **6**, 1629–1633.

33 C. N. Lim, C. Kantaridis, I. Huyghe, D. Gorman, S. Berasi and G. E. Sonnenberg, A Phase 1 first-in-human study of the safety, tolerability, and pharmacokinetics of the ROBO2 fusion protein PF-06730512 in healthy participants, *Pharmacol. Res. Perspect.*, 2021, **9**, e00813.

34 Y. Vugmeyster, X. Xu, F. P. Theil, L. A. Khawli and M. W. Leach, Pharmacokinetics and toxicology of therapeutic proteins: Advances and challenges, *World J. Biol. Chem.*, 2012, **3**, 73–92.

35 M. P. Baker, H. M. Reynolds, B. Lumicisi and C. J. Bryson, Immunogenicity of protein therapeutics: The key causes, consequences and challenges, *Self Nonself*, 2010, **1**, 314–322.

36 V. Jawa, F. Terry, J. Gokemeijer, S. Mitra-Kaushik, B. J. Roberts, S. Tourdot and A. Groot, T-Cell Dependent Immunogenicity of Protein Therapeutics Pre-clinical Assessment and Mitigation-Updated Consensus and Review 2020, *Front. Immunol.*, 2020, **11**, 1301.

37 S. Song, L. Yang, W. L. Trepicchio and T. Wyant, Understanding the Supersensitive Anti-Drug Antibody Assay: Unexpected High Anti-Drug Antibody Incidence and Its Clinical Relevance, *J. Immunol. Res.*, 2016, **2016**, 3072586.

38 T. S. Maurer, M. Edwards, D. Hepworth, P. Verhoest and C. M. Allerton, Designing small molecules for therapeutic success: A contemporary perspective, *Drug Discovery Today*, 2022, **27**, 538–546.

39 C. Oo and S. S. Kalbag, Leveraging the attributes of biologics and small molecules, and releasing the bottlenecks: a new wave of revolution in drug development, *Expert Rev. Clin. Pharmacol.*, 2016, **9**, 747–749.

40 S. A. Abdel-Rahman and M. T. Gabr, Optimization and development of a high-throughput TR-FRET screening assay for SLIT2/ROBO1 interaction, *SLAS Discovery*, 2025, **34**, 100240.

41 A. R. Goodnow, C. E. Dumelin and A. D. Keefe, DNA-encoded chemistry: enabling the deeper sampling of chemical space, *Nat. Rev. Drug Discovery*, 2017, **16**, 131–147.

42 A. A. Peterson and D. R. Liu, Small-molecule discovery through DNA-encoded libraries, *Nat. Rev. Drug Discovery*, 2023, **22**, 699–722.

43 A. L. Satz and W. Cui, Analysis of DNA-Encoded Library Screening Data: Selection of Molecules for Synthesis, *Methods Mol. Biol.*, 2022, **2541**, 195–205.

44 P. Ma, S. Zhang, Q. Huang, Y. Gu, Z. Zhou, W. Hou, W. Yi and H. Xu, Evolution of chemistry and selection technology for DNA-encoded library, *Acta Pharm. Sin. B*, 2024, **14**, 492–516.

45 S. Wang, X. Shi, J. Li, Q. Huang, Q. Ji, Y. Yao, T. Wang, L. Liu, M. Ye, Y. Deng, P. Ma, H. Xu and G. Yang, A small molecule selected from a DNA-encoded library of natural products that binds to TNF-a and attenuates inflammation in vivo, *Adv. Sci.*, 2022, **9**, e2201258.

46 P. Ma, H. Xu, J. Li, F. Lu, F. Ma, S. Wang, H. Xiong, W. Wang, D. Burrato, F. Zonta, N. Wang, K. Liu, T. Hua, Z.-J. Liu, G. Yang and R. Lerner, Functionality-independent DNA encoding of complex natural products, *Angew. Chem., Int. Ed.*, 2019, **58**, 9254–9261.

47 C. Morlot, N. M. Thielens, R. B. Ravelli, W. Hemrika, R. A. Romijn, P. Gros, S. Cusack and A. A. McCarthy, Structural insights into the Slit-Robo complex, *Proc. Natl. Acad. Sci. U. S. A.*, 2007, **104**, 14923–14928.